Available online at www.sciencedirect.com
SCIENCE DIRECT®
Journal of Solid State Chemistry 179 (2006) 278–288
JOURNAL OF SOLID STATE CHEMISTRY
www.elsevier.com/locate/jssc

# Structural studies on $W^{6+}$ and $Nd^{3+}$ substituted $La_2Mo_2O_9$ materials

David Marrero-López[a], Jesús Canales-Vázquez[b,c], Wuzong Zhou[c], John T.S. Irvine[c], Pedro Núñez[a,*]

[a]Departamento de Química Inorgánica, Universidad de La Laguna, E38200 La Laguna, Tenerife, Canary Islands, Spain
[b]Instituto de Ciencia de Materiales de Barcelona, ICMAB-CSIC, Campus UAB, 08193 Bellaterra, Spain
[c]School of Chemistry, Purdie Building, University of St Andrews, St Andrews, Fife KY16 9ST, UK

Received 23 August 2005; received in revised form 18 September 2005; accepted 14 October 2005
Available online 17 November 2005

**Abstract**

The structure of a series of new ionic conductors based in lanthanum molybdate ($La_2Mo_2O_9$) has been investigated using transmission electron microscopy (TEM), high-resolution X-ray diffraction (XRD) and differential scanning calorimetry (DSC). The superstructure $2a_c \times 3a_c \times 4a_c$ of the low temperature $\alpha$-polymorph relative to the $\beta$-polymorph was confirmed by HRTEM imaging and electron diffraction. Furthermore, the effects of partial cation substitution in the $La_{2-x}Nd_xMo_2O_9$ and $La_2Mo_{2-y}W_yO_9$ series have been also evaluated in the search of new clues to understand the structure and stabilisation of the high temperature and better conductor $\beta$-polymorph. The thermal analysis studies show that Nd-substitution does not stabilise completely the $\beta$-polymorph at room temperature, although no superstructure ordering was observed by both XRD and HRTEM. On the other hand, W-substitution stabilises the cubic $\beta$-polymorph for $y > 0.25$, although, electron diffraction indicates a slight distortion from the cubic symmetry for low W-content. This distortion disappears as the W content increases and the Rietveld refinements gradually render better results.


*Keywords:* $La_2Mo_2O_9$; Ionic conductor; HRTEM; Superstructure; Phase transition

## 1. Introduction

Oxide ion conductors are materials with a number of important applications such as oxygen sensors, dense ceramics for oxygen separation and fuel cell components. Fuel cells are electrochemical devices that convert directly chemical energy into electricity and promise important advantages in comparison to the current technologies based on the combustion of fossil fuels, because they are environmentally friendly and render higher efficiencies [1–4].

Fuel cells require materials exhibiting high ion oxide mobility, which in turn implies very specific structural features only met for a restricted number of solids. The most widely used solid electrolyte nowadays is yttria-stabilised zirconia (YSZ), which is a very good oxide ion conductor at high temperature (typically $0.1\,S\,cm^{-1}$ at 1273 K) and stable for prolonged operation times [5]. However, the high operation temperatures (1000–1273 K) limit the choice of stable materials for the other SOFC components, hence increasing the costs of production.

Over the last two decades, other ionic conductors such as rare-earth doped ceria and $LaGaO_3$-based phases have been studied and developed based upon fluorite or perovskite structures, respectively, showing higher conductivity than YSZ at lower temperatures [6–10]. Unfortunately, they present other drawbacks such as high cost or residual electronic conductivity that must be overcome. Therefore, an electrolyte with very high conductivity at relatively low temperatures is highly demanded to produce efficient fuel cells operating at intermediate temperatures (IT-SOFCs).

Since the discovery of very high oxide-ion conductivity in $La_2Mo_2O_9$ by Lacorre et al., much attention has been directed towards molybdate-based materials due to their potential applications as electrolyte [11]. This compound was first synthesised by Fournier et al. in 1970 [12],

*Corresponding author. Fax: +34 92 2318461.
*E-mail address:* pnunez@ull.es (P. Núñez).

0022-4596/$ - see front matter © 2005 Elsevier Inc. All rights reserved.
doi:10.1016/j.jssc.2005.10.017

although the reports on the structural characterisation and the high ionic conductivity are more recent [13,14]. The very high oxide ion conductivity in $La_2Mo_2O_9$ has been explained using the lone pair substitution (LPS) concept, which considers that the partial substitution of lone-pair cations by other cations without lone-pair electrons may generate intrinsic-vacancies in the anionic sublattice [15].

$La_2Mo_2O_9$ undergoes a structural phase transition from the slightly monoclinic $\alpha$-polymorph to the much better conductor cubic $\beta$-polymorph (isostructural to $\beta$-$SnWO_4$) at 833 K. This transition is similar to those reported in other fast ionic conductors such as $Bi_2O_3$ and $Bi_2V_4O_{11}$ and is usually associated to a rearrangement in the oxygen sublattice [16,17].

The applicability of $La_2Mo_2O_9$ is limited by the $\alpha \leftrightharpoons \beta$ phase transition and by its stability under reducing conditions. The partial substitution of either $La^{3+}$ or $Mo^{6+}$ by cations such as $Bi^{3+}$, $Ca^{2+}$, $Sr^{2+}$, $Y^{3+}$ and $W^{6+}$ seems to stabilise the cubic polymorph at room temperature, whilst $Nd^{3+}$ has been reported to adopt the monoclinic superstructure [14,18–22]. Recent reports suggest that $La_2Mo_{2-x}W_xO_9$ phases can be used as SOFC electrolytes, although only at low temperature and under moderate reducing conditions. The introduction of tungsten enhances the stability range and prevents the presence of residual electronic conductivity [23–26].

In the present work, $La_2Mo_2O_9$, $(La,Nd)_2Mo_2O_9$ and $La_2(Mo,W)_2O_9$ phases have been studied by high resolution X-ray diffraction (XRD), transmission electron microscopy (TEM) and thermal analysis to give a further insight of these structures.

## 2. Experimental

The synthesis of $La_2Mo_2O_9$ (LMO), $La_2Mo_{2-y}W_yO_9$ (LMW) and $La_{2-x}Nd_xMo_2O_9$ (LNM) series was carried out using a freeze-dried precursor method. The starting materials were $La_2O_3$, $Nd_2O_3$ (99.99% Aldrich), $WO_3$ and $MoO_3$ (99.5% Aldrich). The experimental procedure for the preparation of the freeze-dried precursor powders has been described in detail in previous publications [16,27]. Lanthanum and neodymium oxides were dissolved in diluted nitric acid, and tungsten and molybdenum in diluted ammonia. The solutions were mixed in stoichiometric ratios and then cooled in liquid nitrogen and freeze-dried for 2 days.

A single phase can be obtained after the calcination of the dried precursor powders in air at 673–773 K, although in the present work all samples were calcined between 1123 and 1273 K for 5 h to obtain high crystallinity and to facilitate the structural characterisation. Samples were cooled slowly, i.e. 1–2 K/min in air, to obtain the targeted oxygen stoichiometry and the crystal lattice as close as possible to the equilibrium conditions at room temperature. The samples are labelled as LMO for $La_2Mo_2O_9$ and "Ndx" and "Wy" for $La_{2-x}Nd_xMo_2O_9$ and $La_2Mo_{2-y}W_yO_9$ series, respectively.

XRD patterns were obtained from a Philips X′Pert Pro automated diffractometer, equipped with a primary monochromator and an X′celerator detector. The scans were performed in high resolution mode in the $2\theta$ range from 5° to 120° (step 0.0085–0.016° and 100–500 s/step), using copper $K_{\alpha 1}$ radiation. High-temperature XRD studies were carried out in air, using an Anton Paar TTK 450 Camera, ranging from room temperature to 1123 K. Rietveld refinement of the XRD patterns were performed using FULLPROF software [28]. The fits were performed using a pseudo-Voigt peak-shape function. In the final cycles, the usual profile parameters (scale factors, background coefficients, zero-points, half-width, pseudo-Voigt and asymmetry parameters for the peak-shape) were refined. The occupation numbers and isotropic temperature factors were refined separately due to their strong correlation. All graphics related with XRD patterns were performed using WinPLOTR software [29].

Selected area electron diffraction (SAED) and HRTEM imaging were performed on a JEOL JEM 2011 electron microscope equipped with a ($\pm 20°$) double-tilt sample holder operating at 200 kV. The equipment used an Oxford Link detector to perform EDS analysis. Samples for TEM observation were prepared by dispersion of a very fine ground powder specimen onto a perforated carbon film supported on a Cu grid. Image simulation was carried out using MacTempas software (v. 3.1.1).

Thermal analysis TG/DTA, differential scanning calorimetry (DSC) and dilatometric measurements were recorded with Perkin Elmer Instruments (Pyris Diamond series) in static air at heating/cooling rate of 5–20 K/min.

Dense pellets of 10 mm diameter and 2 mm thick were pressed at 100 MPa and sintered at 1223–1373 K for 5 h for the electrical characterisation. The relative density of these pellets was higher than 98%. Some reference specimens of commercial yttria stabilised zirconia (8%YSZ, Tosoh) and gadolinium-doped ceria (CGO, Rhodia) were also prepared into pellets and sintered at 1673 and 1773 K, respectively for 10 h. A sample of $La_{1.9}Sr_{0.1}Ga_{0.8}Mg_{0.2}O_{2.8}$ was also prepared by solid-state reaction and sintered at 1673 K for 10 h. The overall electrical conductivity was measured by impedance spectroscopy, using a 1260 Solartron frequency response analyser in the frequency range from 0.1 Hz to 1 MHz and temperature range from 573 to 1173 K. All samples were measured in the same environmental conditions to compare their conductivity values. The experimental details are reported elsewhere [23,24].

## 3. Results and discussion

### 3.1. XRD characterisation

As mentioned in the introduction, it is well known that $La_2Mo_2O_9$ undergoes a phase transition from the monoclinic $\alpha$-polymorph to the cubic $\beta$-$La_2Mo_2O_9$ at 833 K, which is accompanied by a great enhancement of

the oxide-ion conductivity. Therefore, it is a priority to find the means of stabilising the high temperature polymorph, which can be achieved by substituting partially $La^{3+}$ and $Mo^{6+}$ by other cations such as $Nd^{3+}$ or $W^{6+}$ as reported in the literature [18–20].

Previous investigations mainly from Goutenoire et al. concluded that the high temperature $\beta$-polymorph presents a cubic symmetry (s.g. $P2_13$) with cell parameter $a_c \approx 7.20$ Å at 890 K [14]. On the other hand, the low temperature $\alpha$-polymorph has been described as a $2a_c \times 3a_c \times 4a_c$ superstructure of the $\beta$-polymorph with a very subtle monoclinic distortion based on electron and neutron diffraction data [13,14]. The structure of $\alpha$-polymorph, including atomic positions has been resolved recently from single crystals, confirming the previous results [30]. Indeed, and as shown in Fig. 1, most of the diffraction peaks show splitting that indicates a monoclinic distortion, accompanied by small 'extra' reflections, which are due to the superstructure (inset Fig. 1). Therefore, the $\alpha$-polymorph can be indexed as having a monoclinic unit cell, (s.g. $P2_1$) with $a = 14.28277(6)$ Å, $b = 21.4533(1)$ Å, $c = 28.6244(1)$ Å and $\beta = 90.4439(2)^\circ$. The corresponding Rietveld refinements match the experimental results reasonably well, which is in complete agreement with the data reported in the literature [13,14,30].

The extra peaks observed in the $\alpha$-polymorph disappear gradually upon the introduction of W in the Mo-sites (Fig. 2a). Thus, for W contents higher than $y = 0.25$ (W0.25) the only reflections observed correspond to the $\beta$-polymorph, which seems to indicate that the stabilisation

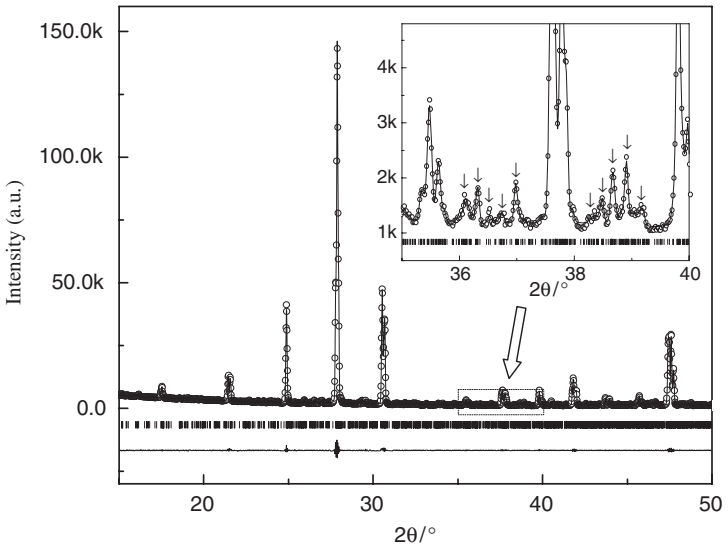


Fig. 1. Selected area of the XRD Rietveld refinement corresponding to the low temperature $\alpha$-polymorph of $La_2Mo_2O_9$ at room temperature. The inset shows some additional reflections compared to the $\beta$-polymorph (marked with arrows) that fitted reasonably well in the $P2_1$ space group.

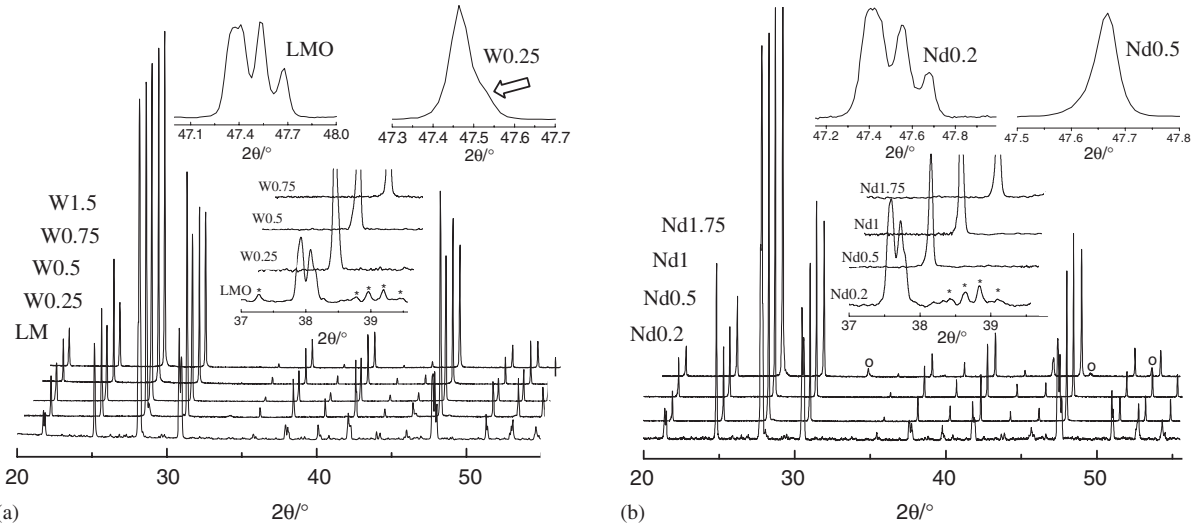


Fig. 2. XRD patterns of: (a) $La_2Mo_{2-y}W_yO_9$ and (b) $La_{2-x}Nd_xMo_2O_9$ series. Some impurity peaks appear for neodymium composition higher than Nd1.5 (o). The inset shows the evolution of the (231) reflection and the vanishing of the small additional reflections (*) of the $\alpha$-polymorph with the W or Nd content.

has been achieved at room temperature. However, it should be noted that for tungsten contents lower than $y = 0.25$ (W0.25) the XRD peaks are asymmetric (inset Fig. 2a), which might indicate that the two polymorphs coexist at low W contents due to a gradual change in the phase distribution as the two-phase region is traversed. Indeed, the cell parameters evolve with W reaching a maximum for W0.5 and decrease upon further substitution to W1.5 (Fig. 3). This deviation from Vegard's law could possibly indicate the existence of a structural change. At higher tungsten content, W1.8, a triclinic phase isostructural with $La_2W_2O_9$ is stabilised [31].

The results were analogous for the $La_{2-x}Nd_xMo_2O_9$ (LNM) system. At Nd content higher than $x = 0.5$ (Nd0.5) no additional reflections compare to the $\beta$-polymorph are observed (Fig. 2b). It should be stressed that Nd could substitute up to 1.75 La per formula unit, rendering nearly single phases. Minor impurity diffraction peaks of a non-identified phase were observed for Nd content higher than $x = 1.5$ (Nd1.5). The intensity of the impurity peaks increase gradually with the Nd content and they also appear for samples with lower Nd-content, when the samples were synthesised at temperatures above 1223 K. Furthermore, the cell parameters decrease linearly with increasing the Nd content (i.e. following Vegard's law) in good agreement with the rare earth ionic radii (116.3 Å for Nd and 121.6 Å for La [32]) (Fig. 3). The substitution limit found in the present work is higher than that found by Georges et al. [20], where the maximum Nd acceptance was only Nd1.0. The main reason might be the different synthesis method used and taking into account that the phases investigated in the present article were obtained at much lower temperatures and shorter reaction time.

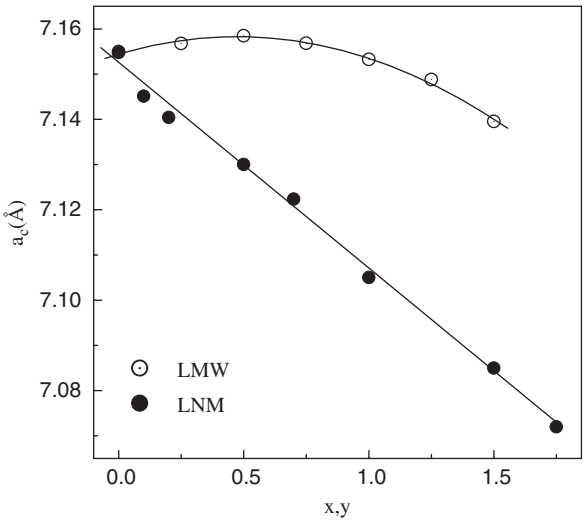


Fig. 3. Variation of the cubic lattice parameter, $a_c$, for $La_2Mo_{2-y}W_yO_9$ (○) and $La_{2-x}Nd_xMo_2O_9$ (●) series as a function of both tungsten and neodymium concentration.

The Rietveld refinements corresponding to the LMW and LNM phases were carried out using the models proposed by Goutenoire et al. for the $\beta$-polymorph, based on neutron diffraction data [13]. The best results were obtained considering full occupation of the La, Mo and O1 sites, whereas the O2 and O3 sites responsible for the ionic conductivity are partially occupied (81% and 34%, respectively) as shown in Fig. 4 and Table 1. It should be noted that the atomic positions and occupancies are similar to those reported for $\beta$-$La_2Mo_2O_9$, although the error associated to the oxygen atoms is high due to the dominant scattering power of the heavy cations. The refinement results seem reasonably good, although one should notice the very high thermal factors. This was first interpreted to be a consequence of the very high mobility of the oxygen in this structure [13]. However this explanation is not fully satisfactory as the metal cations also presented abnormally high thermal factors. Indeed, the $R$-factors are rather high for all of the Nd substituted series ($R_F = 8.3$, $R_B = 5.8$ and $R_{wP} = 10.7$ for Nd1) as well as in specimens with low W content ($R_F = 10.4$, $R_B = 9.5$ and $R_{wP} = 9.6$ for W0.5), improving as the W content increases (Table 1). This possibly indicates that the phases with low levels of substitution present a slight distortion from the cubic symmetry. One should note that some peaks are clearly asymmetric especially for the LNM system (inset Fig. 4b),

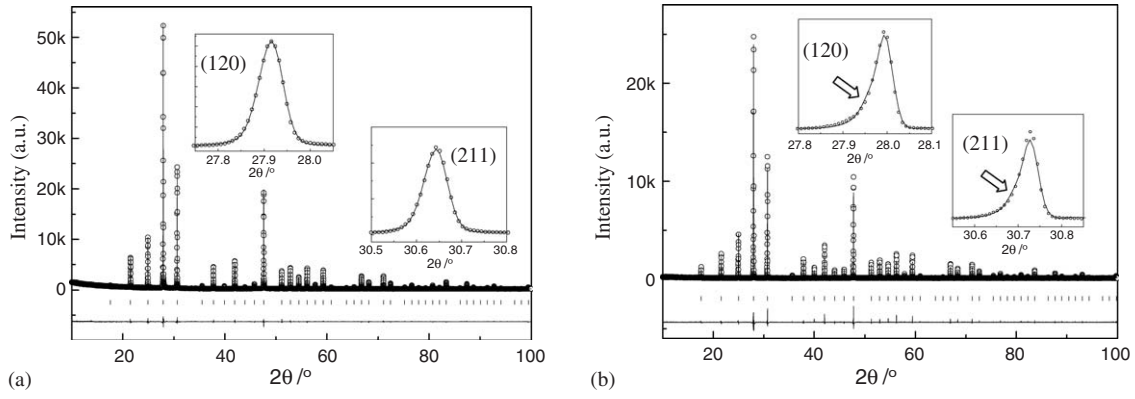


Fig. 4. Rietveld refinement for: (a) $La_2Mo_{0.5}W_{1.5}O_9$ and (b) $LaNdMo_2O_9$ phases, showing experimental (circles), calculated (continuous line), and difference profiles. The insets show the fitting of some diffractions peaks. Asymmetric peaks are observed for $LaNdMo_2O_9$, indicating a possible small distortion of the cubic cell.

Table 1
Structural parameters for $La_2Mo_{0.5}W_{1.5}O_9$ in space group $P2_13$

| Atom/Wyckoff site | $x$ | $y$ | $z$ | Occ. | $B_{iso}$ |
|---|---|---|---|---|---|
| $La_2Mo_{0.5}W_{1.5}O_9$ ($a = 7.13952(2)$ Å) | | | | | |
| La(4*a*) | 0.8581(1) | 0.8581(1) | 0.8581(1) | 1.00 | 3.9(5) |
| Mo/W(4*a*) | 0.1659(1) | 0.1659(1) | 0.1659(1) | 0.25/0.75 | 4.7(1) |
| O1(4*a*) | 0.328(1) | 0.328(1) | 0.328(1) | 1.00 | 9.2(5) |
| O2(12*b*) | 0.986(2) | 0.203(1) | 0.383(2) | 0.80(4) | 6.4(7) |
| O3(12*b*) | 0.893(3) | 0.694(3) | 0.589(3) | 0.34(3) | 4.1(9) |

$R_p$: 4.9; $R_{wp}$: 6.7; $R_{exp}$: 5.0; $\chi^2$: 1.76, $R_B$: 2.95; $R_F$: 5.71.

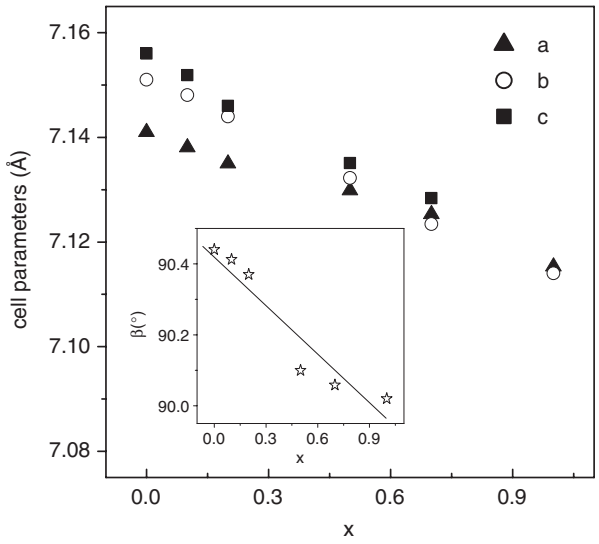


Fig. 5. Variation of cell parameters considering a monoclinic unit cell as a function of the Nd content. The cell parameters become closer to cubic as the Nd content increases.

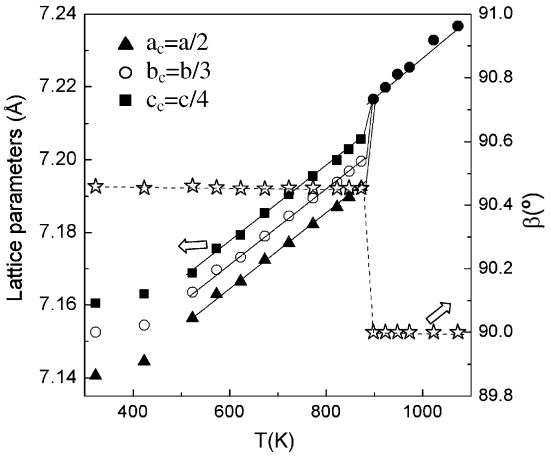


Fig. 6. Thermal evolution of the lattice parameters of $La_2Mo_2O_9$, indexed as monoclinic and cubic unit cells below and above the phase transition temperature, respectively.

becoming gradually smaller with increasing the W or Nd content, which in turn implies that the introduction of such cations renders phases gradually closer to the cubic. This also seems to indicate that there exists a subtle distortion from the cubic unit cells for tungsten contents lower than W0.5 and for all of the Nd-doped samples. Refinements considering monoclinic unit cells were performed and although the results compared to those with a cubic unit cell were not significantly improved, they showed a rather clear trend of unit cell parameters becoming closer to cubic as more W and Nd was introduced in the structure (Fig. 5).

### 3.2. High temperature XRD

The XRD patterns at different temperatures for $La_2Mo_2O_9$ were indexed as monoclinic for the α-polymorph (s.g. $P2_1$) and cubic (s.g. $P2_13$) for the β-polymorph below and above the phase transition temperature, respectively (Fig. 6). The low temperature α-polymorph was indexed without taking into account the small reflections due to superstructure and considering only the monoclinic distortion relative to the β-polymorph. As can be observed, the cell parameters increase nearly linearly with the temperature. Additionally, the monoclinic angle for the α-polymorph remains constant in the low temperature range (~90.46°), similar results were obtained by Georges et al. [30].

The thermal evolution of cell volume for $La_2Mo_2O_9$ reveals a clear deviation at the phase transition temperature, where an important increase rate of the cell, ~0.5% in volume per 25 K of temperature increase, can be observed (Fig. 7). Besides, the peaks splitting and small additional reflections vanish above the phase transition temperature (Inset Fig. 7). A small hysteresis is also observed during the heating–cooling process, indicating a first-order phase transition as confirmed by DSC, electrical and dilatometric measurements [16].

In the LMW system (Fig. 7), there are not drastic changes in the cell volume, but a certain discontinuity at ~800 K can be observed as the behaviour cannot be described by a straight line. It should be mentioned that this discontinuity is reminiscent of those reported for stabilised δ-$Bi_2O_3$ and γ-$Bi_2V_4O_{11}$ electrolytes, where the discontinuity on heating is mainly associated with disordering of the oxygen sublattice and also removal of oxygen from the crystal lattice as the temperature increases [17,33]. From these results one would suggest that the phase transition is suppressed by W substitution, although there exists some degree of structural re-arrangement upon heating/cooling.

As for the LNM system, despite the XRD peaks did not split in the whole temperature range studied, the cell

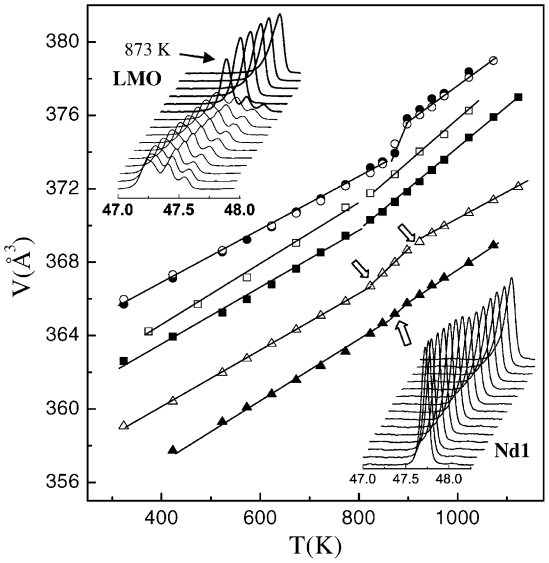


Fig. 7. Thermal evolution of cell volume of $La_2Mo_2O_9$ (○ heating, ● cooling), $La_2Mo_{2-x}W_xO_9$ (□ W0.75 and ■ W1.5) and $LaNdMo_2O_9$ (△ Nd1 and ▲ Nd1.5). LMW shows a subtle discontinuity as the response cannot be described by a straight line. The insets show the variation of (231) reflection as the temperature increases for LMO and Nd1. The peak splitting vanishes above the phase transition temperature for $La_2Mo_2O_9$. That reflection does not split for $LaNdMo_2O_9$ in the whole temperature range, although a discontinuity in the cell parameter is observed around the phase transition temperature, which might imply a slight structural change on heating.

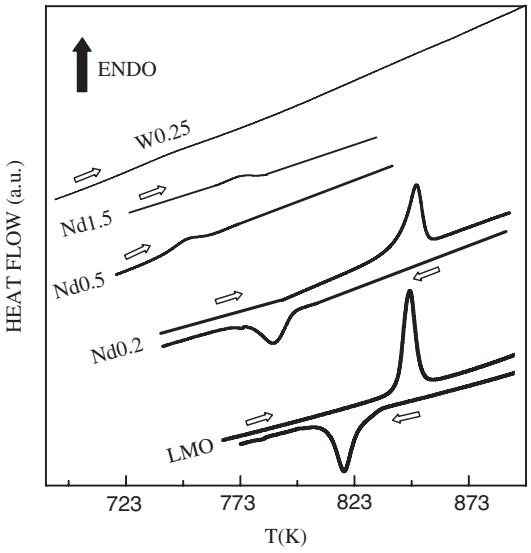


Fig. 8. DSC curves showing the reversible phase transition of $La_2Mo_2O_9$ (LMO) and no complex stabilisation of $\beta$-polymorph for $La_{2-x}Nd_xMo_2O_9$ ($Nd_x$) series. No phase transition is observed for $La_2Mo_{2-y}W_yO_9$ (Wy) series.

volume changes slightly around the phase transition temperature as happened for pure $La_2Mo_2O_9$, although in a broader range of temperature (Fig. 7). The increase of Nd content reduces the change of volume cell at the phase transition temperature and for Nd1.5 it is very small. A possible explanation for this behaviour is that only some crystallites present superstructure after Nd substitution, coexisting the $\alpha$ and $\beta$ polymorphs at low temperature with similar cell parameters and very subtle monoclinic distortion for the $\alpha$-polymorph.

### 3.3. Thermal analysis

The DSC measurements show a clear reversible phase transition for $La_2Mo_2O_9$ with a thermal hysteresis as expected for a first-order transition (Fig. 8). The partial substitution of $La^{3+}$ by $Nd^{3+}$ does not seem to suppress completely the phase transition as shown in Fig. 8. The phase transition peak becomes smaller and wider with increasing the Nd-content, although it is still present at high Nd-contents. This seems to indicate that the cubic phase is not entirely stabilised when $Nd^{3+}$ replaces partially $La^{3+}$. The gradual lower enthalpy change calculated by numerical integration of the recorded DSC thermal curves (after the correction for the calorimetric base line) takes values ranging from 5.3 kJ/mol for LMO to 0.6 kJ/mol for Nd1.5. This implies that the transition for the Nd series is rather subtle in comparison with the well-defined monoclinic $\alpha$- to cubic $\beta$-form in $La_2Mo_2O_9$, because possibly only a minor fraction of crystallites shows superstructure ordering.

On the other hand, no peak attributable to a phase transition was observed for the W-substituted phases in the temperature range studied, indicating that the $\beta$-polymorph is stabilised at room temperature. This result is apparently contrary to the XRD results that highlighted the presence of asymmetric peaks for samples with low W content and consequently the not fully satisfactory Rietveld refinement using a cubic unit cell. One would suggest that the enthalpy change in the present case is so small that it lies beyond the resolution limit of the technique.

### 3.4. TEM characterisation

#### 3.4.1. $\alpha$-$La_2Mo_2O_9$

Preliminary results of electron diffraction confirmed the $2\times3\times4$ superstructure previously reported for the $\alpha$-polymorph as shown in Fig. 9. It should be noted that on the SAED patterns corresponding to the main zone axes, i.e. [100], [010] and [001], it is relatively easy to detect the slight monoclinic distortion in the cubic subcell arising from the different $d$-spacing and inter-axis angle. The corresponding HRTEM images further confirm the presence of a $2\times3\times4$ superstructure relative to the $\beta$-polymorph (Fig. 9), although sets of perpendicular domains could be observed in some of the crystallites studied in the TEM microscope (Fig. 10).

It should be noted that beam irradiation could also affect the $\alpha$-polymorph under investigation. Fig. 11, shows the HRTEM images corresponding to a view down the [101] zone axis after short (a) and prolonged (b) exposure under the electron beam for an $\alpha$-$La_2Mo_2O_9$ crystallite. The

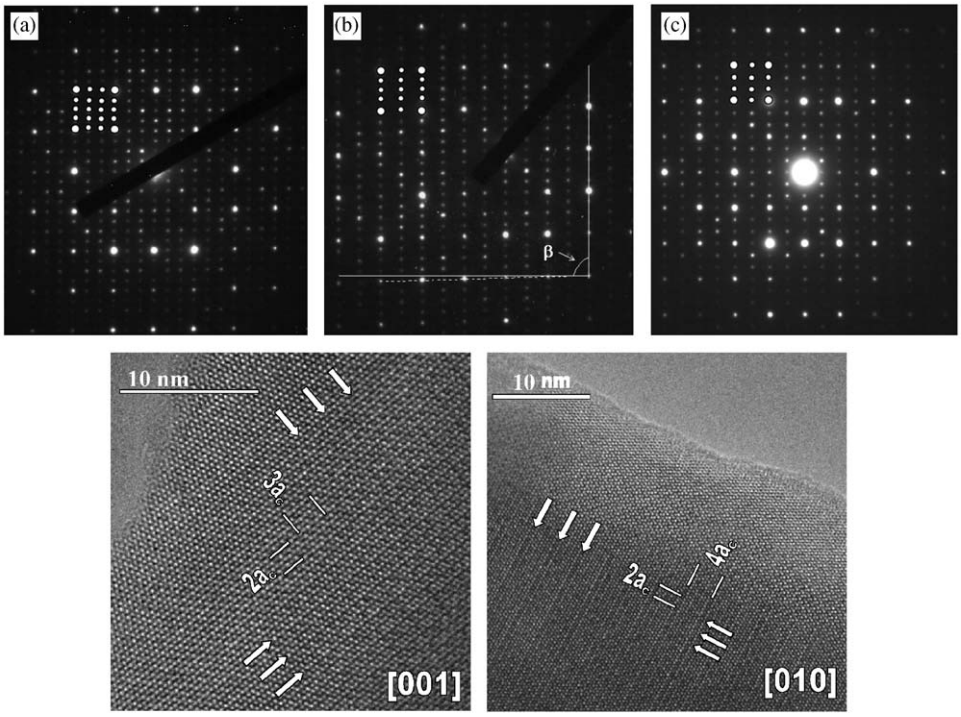


Fig. 9. SAED patterns corresponding to the (a) [100], (b) [010] and (c) [001] zone axes, respectively. The patterns could be indexed considering a $2 \times 3 \times 4$ superstructure of the $\beta$-polymorph with a monoclinic distortion. The diffraction spots are highlighted with large white dots from the $\beta$-type basic unit cell and small ones from the $2 \times 3 \times 4$ supercell. The unit cell parameter, $\beta$, is marked in (b). Bottom: HRTEM images in the [001] and [010] zone axes for the $\alpha$-$La_2Mo_2O_9$, showing very clearly the $2a_c \times 3a_c$ and the $2a_c \times 4a_c$ superstructure, respectively.

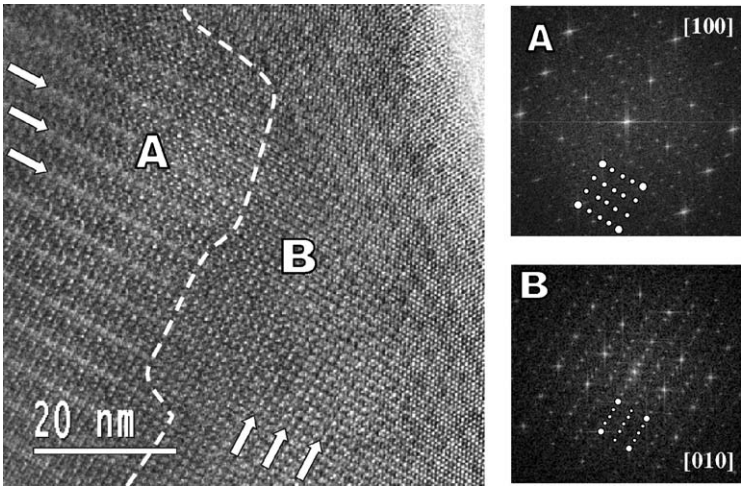


Fig. 10. HRTEM image of $\alpha$-$La_2Mo_2O_9$ showing (A) $3 \times 4$ and (B) $4 \times 2$ perpendicular superstructure domains.

conditions inside the electron microscope presumably promote some reduction that causes the annihilation of the superstructure, i.e. the $\alpha$- to $\beta$-phase transition is favoured inside the TEM microscope.

### 3.4.2. Substituted phases

The substitution of $Mo^{6+}$ by $W^{6+}$ has been reported to be effective at so low levels as W0.3 as suggested by XRD and confirmed by SAED, where the only reflections observed correspond to the cubic cell (Fig. 12a and b) [14,34]. However, in the W-substituted phases (W0.5) the SAED pattern corresponding to the [001] zone axis reveals that the unit cell cannot be treated as cubic, because the inter-axes angle is different from 90.0°. This is not surprising if one considers that $W^{6+}$ and $Mo^{6+}$ have almost the same ionic radius (0.59 Å versus 0.60 Å for $Mo^{6+}$ and $W^{6+}$, respectively) and therefore the substitution should not affect largely the structure for low W content. Further W-substitution decreases the degree of distortion and thus, for the W1.5 phase, the monoclinic

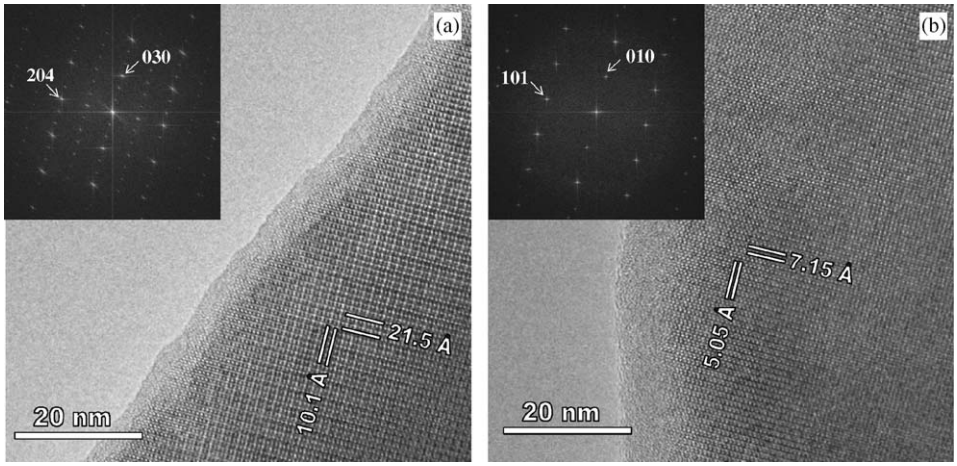


Fig. 11. HRTEM images showing a view down the [101] of a cubic unit cell zone axis after (a) short and (b) prolonged exposure under the electron beam, producing a transformation of $\alpha$ to $\beta$-polymorph. The inset shows the corresponding FFT of the image recorded with the CCD camera.

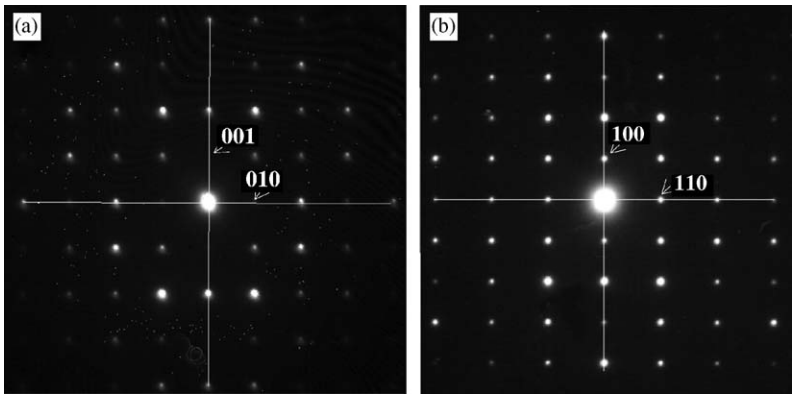


Fig. 12. SAEDs patterns of: (a) W0.5 and (b) W1.5 phases, corresponding to a view down the [010] and [$\bar{1}$10] direction, respectively. The *d*-spacings of (001) and (100) are different and the inter-axis angle is not exactly 90.0° for W0.5, indicating a possible slight monoclinic distortion. The distortion becomes gradually smaller as the tungsten content increases and it is indiscernible for W1.5 phase. (Solid lines have the same length and they are perpendicular.)

distortion is undiscernible. These results agree with the better fitting parameters obtained during the Rietveld refinement of phases with higher W content.

The $La_{2-x}Nd_xMo_2O_9$ phases are especially interesting to understand the stabilisation of the $\beta$-polymorph in these phases. As mentioned above, there exists some controversy regarding whether substituting La by Nd renders completely cubic phases [20,34,35]. No evidence of superstructure or other sort of longer-distance ordering can be found by SAED at different Nd, higher than Nd0.2 (except for this composition) (Fig. 13), which would be apparently against Georges' results, suggesting that the $2 \times 3 \times 4$ monoclinic supercell is kept upon Nd substitution [20]. Our TEM and XRD results did never show evidences of superstructure formation, although DSC measurements show clearly a phase transition, which suggests that only a minor fraction crystallites exhibits superstructure formation or, more likely, the substituted-phase is not cubic at low temperatures (without superstructure) and undergoes a phase transition upon heating. Indeed, the inter-axes angle of the SAEDs patterns remains different from 90.0° and this distortion decreases as the Nd content increases, rendering nearly cubic phases as observed by XRD.

HRTEM images for W and Nd content samples are shown in Fig. 14. The images do not show superstructure ordering or domains in contrast to the $\alpha$-polymorph in any of the samples studied. The calculated images using the multi-slice method (MacTempas) from the structural data obtained by XRD fitted reasonably well to the experimental image, which indicates that the structural model proposed in the literature is reasonably correct. Nevertheless, some deviations are observed in certain crystallographic axes for the Nd content samples. The positions of the atomic columns are slightly shifted when comparing both images (Fig. 14c), which highlights the presence of a minor deviation from the cubic symmetry as suggested by both XRD and SAED.

### 3.5. Electrical characterisation

The evaluation of the electrical properties might render further information to understand the structure and the

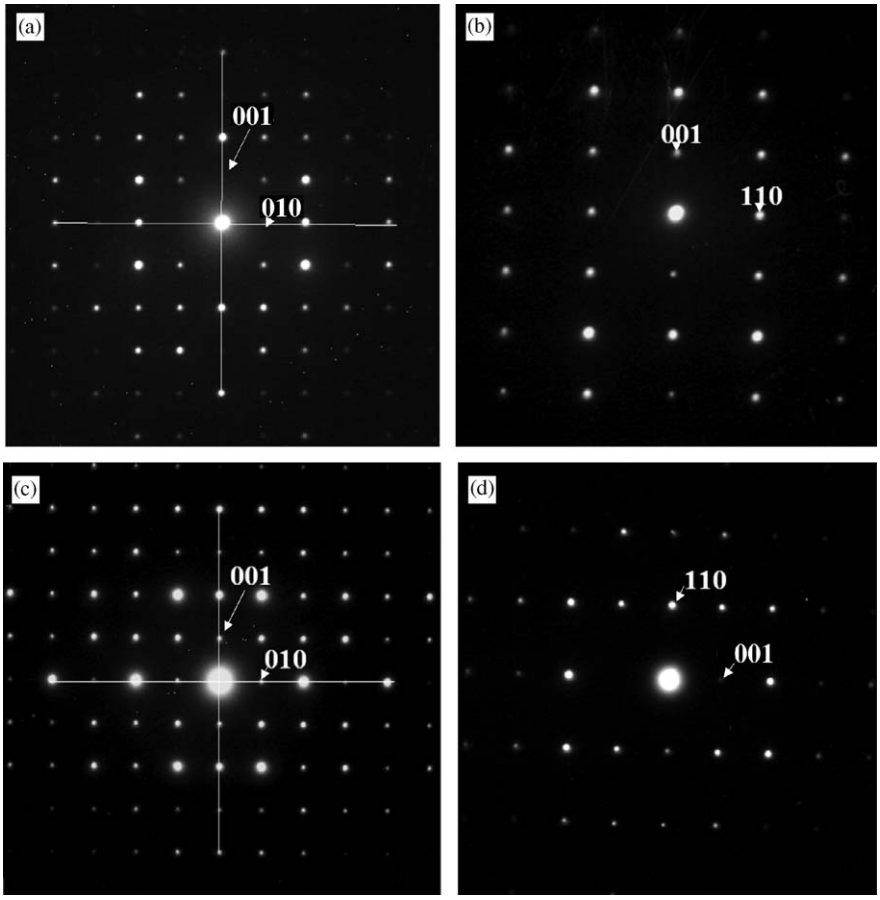


Fig. 13. SAEDs for Nd0.5 samples (a) and (b) and Nd1.5 (c) and (d) in different zone axes.

phase transitions occurring in these phases. As it has been well established, the $\alpha \rightarrow \beta$ phase transition is accompanied by an abrupt increase of the conductivity and therefore it can be used to study the phase transition and stabilisation of the $\beta$-polymorph in the LNM and LMW series.

Impedance spectra plots (Fig. 15a) were analysed with an equivalent circuit $(R_1Q_1)(R_2Q_2)(R_3Q_3)$ consistent in three serial (RQ) elements ascribed to the bulk, grain boundary and electrodes processes, where (RQ) is a resistance and a pseudo-capacitance in parallel. The resistance and capacitance of the different processes were calculated using a non-linear fitting (equivalent circuits) to study the conductivity and the permittivity as a function of the temperature.

The Arrhenius plots corresponding to the overall ionic conductivity for some selected samples of LMW and LNM series are shown in Fig. 15b and compared with the conductivity values obtained for commercial samples of the most important ionic conductor at intermediate temperatures: yttria stabilised zirconia ($Zr_{0.84}Y_{0.16}O_{1.92}$) [36], gadolinium-doped ceria ($Ce_{0.8}Gd_{0.2}O_{1.9}$) [37] and strontium-manganese-doped lanthanum gallate ($La_{1.9}Sr_{0.1}Ga_{0.8}Mg_{0.2}O_{2.85}$) [38]. As can be observed, the conductivity of $La_2Mo_2O_9$ is comparable to these materials above 873 K, where the main contribution to the overall conductivity is due to the grain interior, reaching conductivity values of 0.08 S/cm at 973 K. On the other hand, the conductivity is several orders of magnitude lower, below the phase transition temperature. In addition, Subasri et al. [39] have reported that the values of ionic conductivity in $La_2Mo_2O_9$ are considerably lower compared to the data reported previously by Lacorre et al. [11]. A significant n-type electronic conduction at oxygen partial pressures lower than $10^{-4}$–$10^{-3}$ atm was also indicated by these authors, though recent studies confirmed the high ionic conductivity and negligible electronic conductivity of these materials in a wide range of oxygen partial pressure [23–25,33]. The results found by Subasri et al. could be due to electrode polarisation in the e.m.f. technique used, which leads to an overestimation of the electronic conduction. Furthermore, the microstructure and grain boundary segregations also affect significantly the transport properties of $La_2Mo_2O_9$-based materials as reported elsewhere [27,40].

Tungsten substitution seems to suppress the conductivity drop below the phase transition temperature, whereas in Nd-substituted samples there is no a sharp conductivity enhancement above the phase transition. It should be noted however that for the LNM series there exists certain non-linearity at 788 K. The thermal evolution of bulk permittivity obtained from grain interior contribution shows clearly a peak, which can be ascribed to the phase

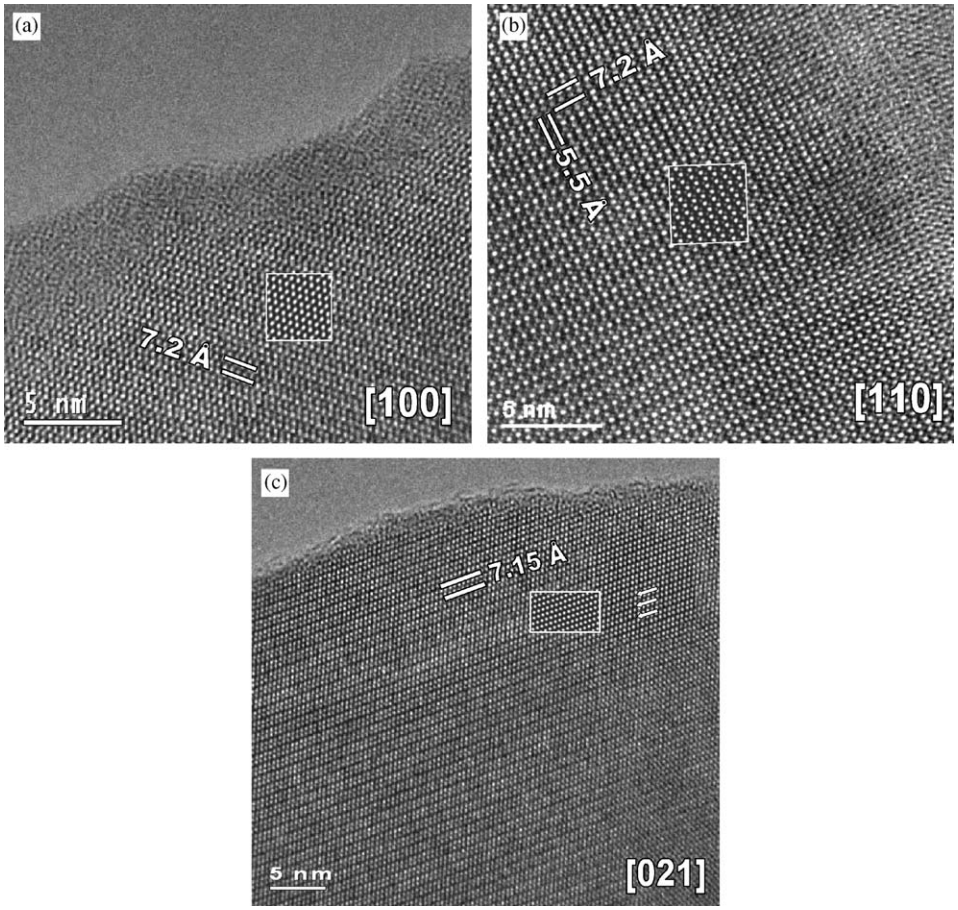


Fig. 14. HRTEM images showing a view down to the (a) [100] for Nd15 (b) [110] for W15 and (c) [021] for Nd0.5. The insets correspond to the simulated image with MacTempas (defocus = 20 Å, thickness = 410 Å for Nd1.5 and Nd0.5, defocus = 25 Å, thickness = 510 Å for W1.5). Small differences in the atom columns are observed for Nd0.5 in the [021] zone axis.

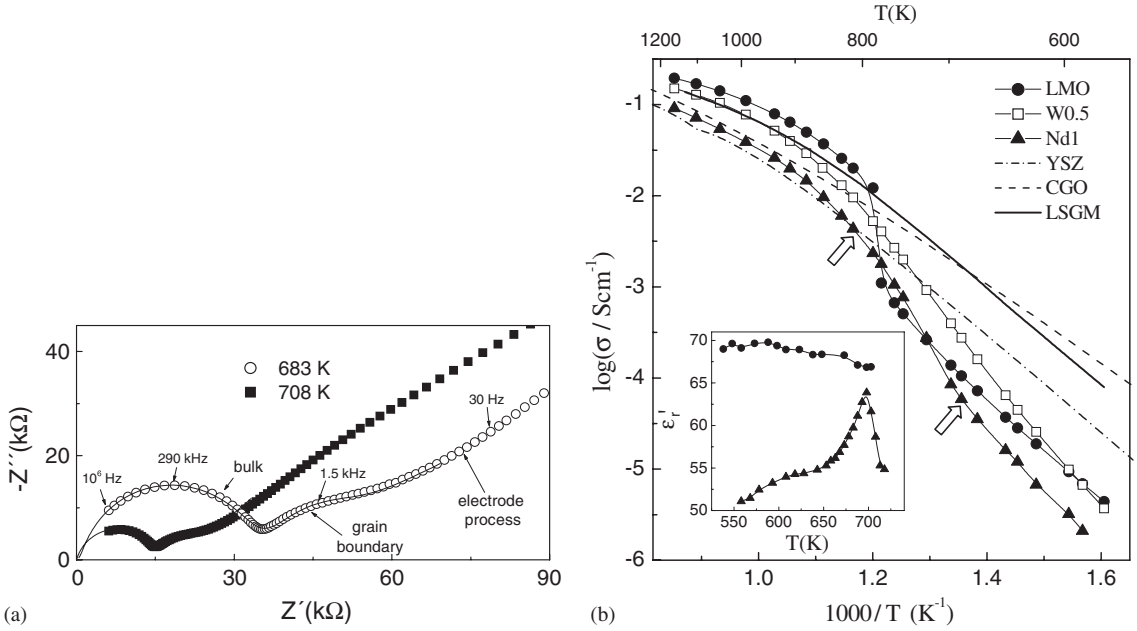


Fig. 15. Nyquist plot for: (a) $LaNdMo_2O_9$ (Nd1) and (b) Arrhenius plot of the overall conductivity for $La_2Mo_2O_9$ (LMO), $La_2Mo_{1.5}W_{0.5}O_9$ (W0.5), $LaNdMo_2O_9$ (Nd1), $Zr_{0.84}Y_{0.16}O_{1.92.}$ (YSZ), $Ce_{0.8}Gd_{0.2}O_{1.9}$ (CGO) and $La_{1.9}Sr_{0.1}Ga_{0.8}Mg_{0.2}O_{2.85}$ (LSGM). The inset of (b) shows the thermal dependence of permittivity of LMO and Nd1.

transition (Inset Fig. 15b). This peak is not observed for $La_2Mo_2O_9$, because the phase transition occurs at higher temperature in good agreement with DSC measurements.

On the other hand, cation substitution used in the present work does not enhance the conductivity of $La_2Mo_2O_9$, which is contrary to the results found in some other works [20,35]. This can be explained as due to the low relative density obtained for $La_2Mo_2O_9$ specimens synthesised via conventional solid-state reaction (80–85%) as discussed in a previous publication [16].

## 4. Conclusions

$Nd^{3+}$ and $W^{6+}$ substituted $La_2Mo_2O_9$ materials have been investigated by XRD, HRTEM and DSC to establish whether the cubic $\beta$-polymorph can be stabilised upon cationic substitution. The substitution of $Mo^{6+}$ by $W^{6+}$ preserving the $La_2Mo_2O_9$ structure is possible up to W1.5, whereas the $La^{3+}$ can be substituted by $Nd^{3+}$ up to Nd1.75.

The $\alpha$-polymorph is a $2\times3\times4$ slightly monoclinic superstructure of the high temperature $\beta$-polymorph, as confirmed both SAED and HRTEM imaging studies. The cationic substitution of $La^{3+}$ by $Nd^{3+}$ does not suppress completely the $\alpha \rightleftharpoons \beta$ phase transition, although no superstructure ordering was observed by XRD or HRTEM. This possibly indicates that only a minor fraction of crystallites gives rise to superstructure. On the other hand, a small monoclinic distortion is observed for specimens with low $W^{6+}$ and $Nd^{3+}$ content. This distortion decreases as the cation substituted increases, rendering nearly cubic phases and improving the Rietveld refinement.

## Acknowledgments

The authors would like to thank the Spanish Research Program MCyT (MAT-2004-3856), Canary Government (PI2004/093), ESF-OSSEP, EPSRC, EU-SOFC Real, for financial support. D. Marrero-López wishes to thank Canary Government and the European Science Foundation (OSSEP-program) for a grant. The authors are also grateful to Judith Oró-Solé (ICMAB-CSIC, Spain) and Dr. Susana García-Martín (UCM, Spain) for their valuable comments on the diffraction data presented in this article.

## References

[1] B.C.H. Steele, A. Heinzel, Nature 414 (2001) 345–352.
[2] J.H. Hirschenofer, D.B. Stauffer, R.R. Engelman, M.G. Klett, Fuel Cell Hanbook, DOE/FETC-99/1076, Morgantown, Fifth ed. 1998.
[3] T. Kudo, in: P.J. Gelling, H.J.M. Bouwmeester (Eds.), The CRC Handbook of Solid State Electrochemistry, CRC Press, Boca Ratón, 1997, p. 195.
[4] B.C.H. Steele, J. Mater. Sci. 36 (5) (2001) 1053–1068.
[5] H. Arai, Bull. Ceram. Soc. Japan 27 (2) (1992) 100–104.
[6] J.C. Boivin, G. Mairesse, Chem. Mater. 10 (1998) 2870–2888.
[7] J.B. Goodenough, A. Manthiram, P. Paramthaman, Y.S. Zhen, Solid State Ionics 52 (1992) 105–109.
[8] T. Ishihara, H. Masuda, Y. Takita, J. Am. Chem. Soc. 116 (9) (1994) 3801–3803.
[9] H. Inaba, H. Tagawa, Solid State Ionics 83 (1996) 1–16.
[10] D.P. Fagg, J.C.C. Abrantes, D. Pérez-Coll, P. Núñez, V.V. Kharton, J.R. Frade, Electrochim. Acta 48 (2003) 1023–1029.
[11] P. Lacorre, F. Goutenoire, O. Bohnke, R. Retoux, Nature 404 (2000) 856–858.
[12] J.P. Fournier, J. Fournier, R. Kohlmuller, Bull. Soc. Chim. Fr. 12 (1970) 4277–4283.
[13] F. Goutenoire, O. Isnard, R. Retoux, P. Lacorre, Chem. Mater. 12 (2000) 2575–2580.
[14] F. Goutenoire, O. Isnard, E. Suard, O. Bohnke, Y. Laligant, R. Retoux, P. Lacorre, J. Mater. Chem. 11 (2001) 119–124.
[15] P. Lacorre, Solid State Sci. 2 (2000) 775–778.
[16] D. Marrero-López, J.C. Ruiz-Morales, P. Núñez, J.C.C. Abrantes, J.R. Frade, J. Solid State Chem. 177 (7) (2004) 2378–2386.
[17] V.V. Kharton, E.N. Naumovich, A.A. Yaremchenko, F.M.B. Marques, J. Solid State Electrochem. 5 (3) (2001) 160–187.
[18] J.A. Collado, M.A.G. Aranda, A. Cabeza, P. Olivera-Pastor, S. Bruque, J. Solid State Chem. 167 (1) (2002) 80–85.
[19] X.P. Wang, Q.F. Fang, S.Z. Li, G.Z. Yi, Appl. Phys. Lett. 81 (18) (2002) 3434–3436.
[20] S. Georges, F. Goutenoire, F. Altofer, D. Sheptyakov, F. Fauth, E. Suard, P. Lacorre, Solid Sate Ionics 161 (3,4) (2003) 231–241.
[21] Q.F. Fang, X.P. Wang, Z.S. Li, G.G. Zhang, Z.G. Yi, Mat. Sci. Eng. A 370 (1–2) (2004) 365–369.
[22] S. Georges, F. Goutenoire, O. Bohnke, M.C. Steil, S.J. Skinner, H.-D. Wiemhöefer, P. Lacorre, J. New Mat. Electr. Sys. 7 (1) (2004) 51–57.
[23] D. Marrero-López, J.C. Ruiz-Morales, D. Pérez-Coll, P. Núñez, J.C.C. Abrantes, J.R. Frade, J. Solid State Electrochem. 8 (9) (2004) 638–643.
[24] D. Marrero-López, J. Canales-Vázquez, J.C. Ruiz-Morales, J.T.S. Irvine, P. Núñez, Electrochim. Acta 50 (22) (2005) 4385–4395.
[25] A. Tarancón, T. Norby, G. Dezanneau, A. Morata, F. Peiró, J.R. Morante, Electrochem. Solid State 7 (10) (2004) A373–A375.
[26] S. Georges, F. Goutenoire, Y. Laligant, P. Lacorre, J. Mater. Chem. 13 (9) (2003) 2317–2321.
[27] D. Marrero-López, J. Canales-Vázquez, J.C. Ruiz-Morales, J.T.S. Irvine, P. Núñez, Solid State Ionics 176 (2005) 1807–1816.
[28] J. Rodríguez-Carvajal, FullProf 2004, version 3.00, Laboratoire Léon Brillouin, CEA-Saclay, France, 2005.
[29] T. Roisnel, J. Rodríguez-Carvajal, WinPLOTR, Laboratoire Léon Brillouin-LCSI, France, 2005.
[30] I.R. Evans, J.A.K. Howard, J.S.O. Evans, Chem. Mater 17 (16) (2005) 4074–4077.
[31] Y. Laligant, A. Le Bail, F. Goutenoire, J. Solid State Chem. 159 (11) (2001) 223–227.
[32] R.D. Shannon, Acta Crystallogr. A 32 (1976) 751.
[33] I.P. Marozau, D. Marrero-López, A.L. Shaula, V.V. Kharton, E.V. Tsipsis, P. Núñez, J.R. Frade, Electrochim. Acta 49 (21) (2004) 3517–3524.
[34] Y. Jianhua, G. Zhongua, W. Zhooyin, Y. Dongstein, Solid State Ionics 176 (5,6) (2005) 523–530.
[35] T. Dah-Shyang, H. Meng-Ju, T. Jang-Chung, L. Hsin-Yi, J. Eur. Cer. Soc. 45 (4) (2005) 481–487.
[36] M. Mori, T. Abe, H. Itob, O. Yamamoto, Y. Takeda, T. Kawahara, Solid State Ionics 74 (3,4) (1994) 157–164.
[37] D. Pérez-Coll, P. Núñez, D. Marrero-López, J.C.C. Abrantes, J.R. Frade, J. Solid State Electrochem. 8 (9) (2004) 644–649.
[38] M. Feng, J.B. Goodenouhg, Eur. J. Solid State Inorg. Chem. 31 (8/9) (1994) 663–672.
[39] R. Subasri, H. Näfe, F. Aldinger, Mater. Res. Bull. 38 (15) (2003) 1965–1977.
[40] S. Georges, F. Goutenoire, P. Lacorre, M.C. Steil, J. Eur. Cer. Soc. 25 (16) (2005) 3619–3627.